9.7 Studies of Arctic Mixed-Phase Clouds from SHEBA/FIRE/ACE: May 1-10 Case Study

P. Zuidema[1]*, B. Baker[2], J. Intrieri[1], P. Lawson[2], S. Matrosov[1], M. Shupe[1]
[1]NOAA Environmental Technology Laboratory, Boulder, CO
[2]Stratton Park Engineering Company, Boulder, CO

1. Introduction

Radiative cloud forcing is an important component of the Arctic climate, with Arctic clouds primarily warming the surface (see, for example, Intrieri et al. (2002)). Recent decades have seen a rapid warming of the Arctic surface (Stone, 1997; Bradley et al., 1993), and an improved understanding of Arctic cloud optical properties is critical if we are to understand Arctic climate change.

One important observation from the Surface Heat Budget of the Arctic (SHEBA; Uttal and co authors (2002)) experiment is that often the clouds present over the SHEBA site will contain both liquid and ice somewhere within the vertical column over the site (Shupe et al., 2001; Intrieri et al., 2002). Many of these clouds can be described as mixed-phase, with liquid and ice coexisting near each other. The presence of liquid water can substantially increase the measured surface infrared flux, especially during the winter months (Intrieri and Shupe, 2002). Other studies also establish the radiative importance of even small amounts of liquid water within ice clouds, such as Hogan et al. (2002).

Despite their importance, mixed-phase clouds are generally difficult to characterize. Measurements from surface-based remote sensors hold the promise of comprehensive documentation, but most prevailing cloud property retrieval techniques are designed for all-ice or all-liquid clouds. In this analysis, radar, lidar, radiometer, and rawinsonde measurements are used to separate the liquid and ice components of a mixed-phase cloud existing from May 1-May 10 at the SHEBA site. In particular, a separate characterization of the liquid and ice cloud optical depth can be derived. Comparisons against aircraft measurements encourage confidence in the surface sensor evaluation.

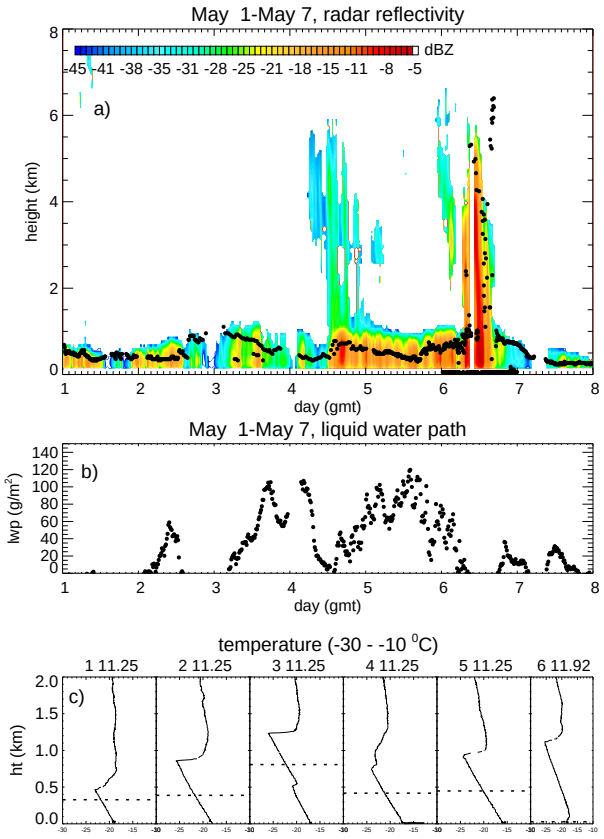

FIG. 1: a) Radar reflectivity in dBZ, with black dots indicating the lidar-determined water cloud bases, b) microwave radiometer-derived liquid water path, and c) sample temperature soundings. Each temperature profile is labeled by day and gmt time. The dashed lines across the temperature profiles indicate the lidar-determined cloud base.

2. Data and Method

2.1 *Data*

Table 1 and 2 list the primary surface-based remote sensors and aircraft datasets utilized within this study. All the surface remote sensors were vertically-pointing. The aircraft data were those available from the May 4, NCAR C-130 plane overflights of the SHEBA site. This was the first FIRE/ACE research flight of the NCAR C-130 aircraft.

* *Corresponding author address:* Paquita Zuidema, NOAA/ETL/ET6, 325 Broadway, Boulder, CO 80305 e-mail:paquita.zuidema@noaa.gov

Table 1: Surface-based instrumentation

Instrument	Vertical Res.	Primary Application	Reference
35 GHz cloud radar	45 m	retrieval of ice component	Moran et al. (1998)
23.8 and 31.8 GHz microwave radiometer	integrated	liquid water path	Westwater et al. (2001)
0.5235 mm polarized micropulse lidar	30 m	cloud phase	Alvarez et al. (1998)
Rawinsondes (2-4 times per day)		pressure, temperature, humidity and winds	

Table 2: Aircraft instrumentation

Instrument	Parameter	Range
FSSP[1]-100	cloud drop and crystal size distribution	2-47 μm particle size
1D OAP[2]-260X	drop and crystal size distribution	40-600 μm
Cloud Particle Imager (CPI)	cloud particle phase, shape, and size	5-2000 μm
King Hot-wire probe	liquid water content	0.05-3 g m^{-3}

[1]Forward scattering spectrometer proble
[2]optical array probe

2.2 *Methodology for the surface-based remote sensors*

A radar-based cloud retrieval technique developed for all-ice clouds can be extended to retrieve the ice component within mixed-phase clouds (Matrosov et al., 2002; Matrosov et al., 2003), with the assumption that the radar is predominantly sensitive to the larger ice particles. The radar-only technique relies solely on radar reflectivity and Doppler velocity to retrieve a vertically-resolved ice water content (IWC), ice mean particle size (D_m), and ice volume extinction coefficient (β). The mean ice particle size is calculated from a quadratic fit to the reflectivity-weighted fall velocity (see Matrosov et al. (2002)). The ice water content is calculated from both the mean particle size and radar reflectivity, and assumes the Brown and Francis (1995) density-size relationship

$$\rho \approx 0.07 D^{-1.1} \qquad (for D > 0.1mm) \qquad (1)$$

A running 20-minute average of the data is created from one-minute data to diminish the influence of larger-scale vertical air motion. Conservative estimates of the IWC and β retrieval errors are a factor of two, and of the D_m retrieval error as 30%. Ice (and liquid) component profiles are established at a ten-minute time resolution.

The vertical profile of the liquid component is derived using a combination of different sensors. The calculation makes use of the observation that liquid water in the Arctic atmosphere is often adiabatically-distributed (see, for example, Lawson et al. (2001)). The lidar can discriminate liquid from ice on the basis of the depolarization ratio - a ratio near zero indicates spherical drops. This is used to establish the water cloud base. An adiabatic liquid water content profile is determined from the lidar-determined cloud base and the temperature structure interpolated from the nearest-in-time soundings. The liquid water path is then constrained using the microwave radiometer-derived liquid water path. Once a liquid water content profile has been established, a volume extinction coefficient profile can be derived using an assumed cloud droplet concentration of 60 cc^{-1}, consistent with retrievals done on all-liquid clouds using a different radar technique (Shupe et al., 2001). Liquid profiles are established whenever lidar data is present and a non-zero microwave radiometer-derived liquid water path exists.

2.3 *Methodology for the in situ data*

Mean microphysical quantities calculated from the aircraft data are compared to the values retrieved from the surface sensors, with separate estimates formed of the complete size distribution for both liquid and ice. First, the best FSSP size distribution was determined. The FSSP-100 probe is known to overestimate liquid water content (LWC) (Lawson et al., 2001), and a correction was applied whereby the FSSP-calculated LWC is decreased to match that measured by the King hot-wire probes. In turn, the King hot-wire probes are known to underestimate liquid water contents, and the King liquid water contents were initially increased by a factor of 1.2, based upon the results of analysis performed at NCAR of the King probe sensor surface area (K. Laursen, pers. comm.). Then, the total CPI size distribution was adjusted to match the FSSP size distribution in regions of overlap. A complete size distribution is then estimated from the FSSP, CPI, and 260X data. The 260X data is known to undercount its smaller particles, and CPI data was preferentially selected in regions of overlap with the 260X data. Thereafter, the size distribution was subsetted into ice and liquid, with all FSSP data assumed to correspond to liquid particles, and the CPI data individually classified into ice and liquid according to a roundness criterium.

The aircraft-derived reflectivity and an ice water content calculation are done using the density-size relationship of Eqn. 1, to be consistent with the retrieval methodology of Matrosov et al. (2002). A separate ice water content calculation is also performed using the methodology of Baker et al. (2002), wherein ice water content is calculated from not only the particle length and width, but also its area and perimeter. The aircraft size distributions were formed from roughly one-minute averages, corresponding to a horizontal distance from the SHEBA site of four km or less, for all but one sample, at 0.96 km, for which a 1.5 minute average corresponding to a horizontal distance of six km and less was utilized.

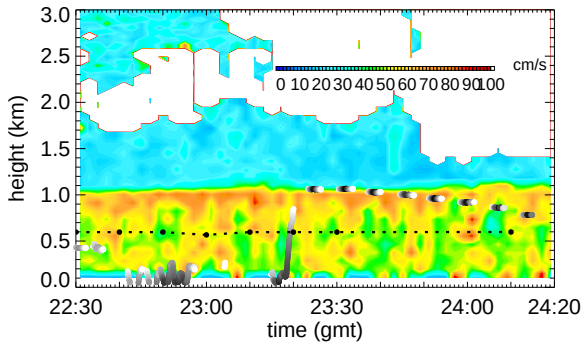

FIG. 2: May 4th aircraft overflights of the SHEBA site projected upon the spectral width of the radar Doppler velocities. Lidar-determined water cloud base shown as a dotted black line. The horizontal distance between the shown aircraft overflights and the SHEBA site are all within ten km, with the smaller horizontal distances shown in darker shades.

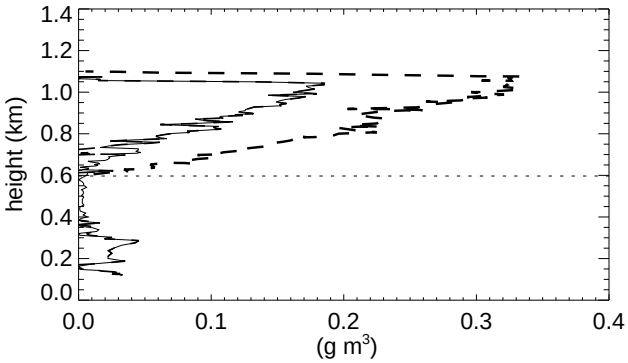

FIG. 3: Liquid water contents (LWCs) measured by the aircraft during its 23:18-23:21 ascent (solid line), and those calculated assuming an adiabatic profile with its base located at the lidar-determined cloud base, and thereafter corrected to match the microwave radiometer-derived liquid water path (dashed line). The dotted line indicates the lidar cloud base.

3. May 1-10 Case Description

The 35 GHz cloud radar reflectivity, lidar-determined water cloud bases, microwave radiometer-derived liquid water path, and selected temperature soundings, all from May 1-7, are shown in Fig. 1. A low cloud persisted throughout the period and two upper clouds came and went. After May 7, the low cloud slowly thinned, dissipating completely on May 10. The radar, lidar, microwave radiometer, and sonde measurements suggest the lower cloud usually contained both ice and super-cooled (temperature $\approx$ -21 °C) liquid. The radar data suggest the upper clouds were ice only, based on high values for the radar Doppler velocities, and low values for the spectral width of the radar Doppler velocities ($<\sim 40$ cm s^{-1}). The presence of the upper clouds coincides with diminished liquid water paths on both May 4th and May 6th. This is suggestive of the Bergeron effect, whereby ice crystals from the upper clouds may be sedimenting into the lower clouds ("seeding") and uptaking the liquid. The liquid water paths increase again after the passage of the upper clouds.

The radar-determined lower cloud top (not shown) usually agreed very well with the location of a 2-3 K temperature inversion; the temperature inversion persisted during the presence of the two upper clouds. The near-surface temperature remained fairly constant at $\sim -18^{\circ}C$, determining the warmest temperatures of the super-cooled liquid. In Fig. 2, the May 4th aircraft overflights of the SHEBA site are shown projected upon the spectral width of the radar Doppler velocities. High values of the radar spectral width can indicate turbulence, but can also serve as an indicator of mixed-phase conditions, with a large spread in Doppler velocities corresponding to a broad distribution of particle sizes.

4. Comparison to aircraft measurements

4.1 *Liquid*

During the 23:18-23:21 aircraft ascent from the near-surface to $\approx$ 1.1 km, one adiabatically-distributed liquid water layer was encountered. The liquid water content profile measured by the aircraft, and that derived from the 23:15 sounding and the lidar-determined cloud base, are shown in Fig. 3. The aircraft-sensed base coincided with the lidar-determined cloud base at 600 m. The adiabatic LWC profile corresponded to a liquid water path of 61 g m^{-2}, close to the microwave radiometer-derived liquid water path at 23:20 of 53.6 g m^{-2}, suggesting that the liquid layer was close to its adiabatic maximum. The aircraft exited the cloud about 12 km away from the SHEBA site, and appears to have encountered less liquid than was present directly over the site.

4.2 *Ice*

Figure 4 shows comparisons between radar-retrieved and aircraft-derived values for a) radar reflectivity, b) ice and liquid water content, c) extinction coefficient, and d) mean ice particle size. Comparisons are shown for six out of the total of eight SHEBA site overpasses; two overpasses, occurring near the top of the liquid cloud, were excluded because little CPI data were collected. The comparisons are more robust below 950 m, where ice concentrations were higher than during the higher overflights.
These conclusions can be drawn from Fig. 4:

- The aircraft reflectivity values derived from the ice particles alone using the Brown and Francis (1995) density-size relationship, are close to the measured radar reflectivities, confirming both that the liquid

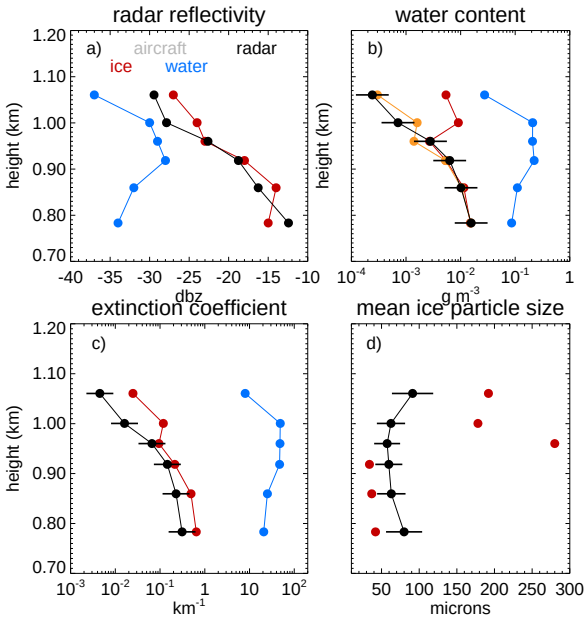

FIG. 4: Comparisons between the radar-retrieved ice microphysics and aircraft-derived microphysical values for liquid and ice of a) reflectivity, b) water content, c) extinction coefficient, and d) mean ice particle size. Radar-retrieved values and their errors are shown in black, values calculated from the aircraft ice and liquid particle size distributions are shown in red and yellow, and blue, respectively. Two different methods for calculating ice water contents from the aircraft data are shown: in red, the method assuming the Brown and Francis (1995) particle density-size relationship, and in dark yellow, the Baker et al. (2002) method.

component contributed negligibly to the radar reflectivity, and that the Brown and Francis (1995) density-size relationship is appropriate.

- The radar retrievals of ice water content compare well to values derived from the aircraft data. For low IWC values (or large mean particle sizes), the method of Baker et al. (2002), wherein the ice particle area and perimeter are considered as well as the particle length and width, appears to agree better with the radar-retrieved IWC values, than the method using Brown and Francis (1995). This may be supported by the overestimate of the aircraft reflectivity values at low dBZ, also done assuming Eqn. 1, that is shown in Fig. 4a. This is a cautious conclusion, however, as the comparison between aircraft and radar is more prone to errors in regions with low IWCs.

- The radar retrieval of the ice volume extinction coefficient appears to be biased slightly low relative to the aircraft-derived values.

- The aircraft mean ice particle sizes are smaller than the radar-retrieved sizes for the lower three overpasses, and greater for the upper three overpasses. This reflects in part the higher ice concentrations present within the lower overpasses, facilitating more robust estimates of the complete size distributions. For the lower three overpasses, the radar retrieval may contain a high bias. For the upper three overpasses, the aircraft size distributions were sparse, with the calculation easily dominated by the presence of only a few large particles. A perusal of the CPI data for the upper overpasses does reveal the presence of several pristine large ice particles, indicating sedimentation from the overlying ice cloud.

- Both the aircraft and radar retrievals of mean ice particle size show an increase towards the cloud top, contrary to theories for the formation of mixed-phase clouds, but again consistent with cloud seeding from above.

5. Liquid and Ice Extinction Coefficients and Optical Depths

The ice vertically-resolved volume extinction coefficients and total ice optical depth are shown in Figure 5. The mean ice cloud optical depth is 0.083, with a maximum of five. An interesting aspect of this figure is the increased values for the extinction coefficient within the lower cloud at times when upper clouds are present. A similar figure is shown for the liquid component in Figure 6, but also includes the liquid effective radius. The effective radius r_e is derived from (Rogers and Yau, 1989):

$$r_e = [\frac{3LWC}{4\pi\rho_w N}]^{1/3} \quad (2)$$

where a droplet concetration N of 60 cc^{-1} is assumed, and ρ_w is the density of liquid water. The liquid optical

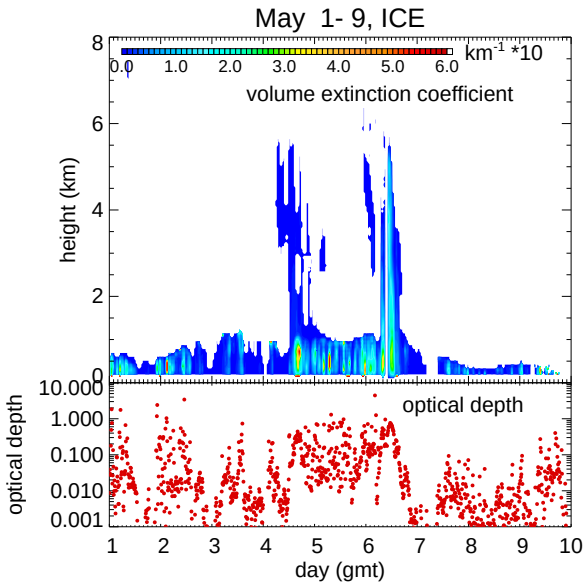

FIG. 5: Radar-retrieved ice volume extinction coefficients (upper panel) and total ice cloud optical depth (lower panel), from May 1-9.

depth usually far surpasses the ice cloud optical depth. The main but indirect radiative influence of the ice is its depletion of the liquid layer on May 6th.

6. Conclusions

Mixed-phase clouds are generally challenging to characterize with current remote sensing technology and retrievals. From May 1-10, 1998, a mixed-phase cloud existed with often high liquid water paths and the presence of ice. For this case, separate characterizations of the ice and liquid components could be done. Aircraft observations on May 4th reveal one, adiabatically-distributed liquid cloud layer. These observations are extended to derive vertical profiles in liquid extinction coefficients consistent with the lidar-determined cloud base and microwave radiometer-derived liquid water path. The aircraft data on ice particles are also compared against the radar ice property retrievals. An important result is that, despite the presence of much larger liquid water contents than ice water contents, the ice component is responsible for almost all of the reflectivity. This supports the extension of radar-only retrievals originally designed for all-ice clouds, to mixed-phase conditions. The radar and aircraft estimates of ice water content and volume extinction coefficient generally show good agreement. The radar retrievals accurately capture the vertical variation of the ice component. Calculations of the ice water content using the method of Baker et al. (2002) may perform better (judged by the comparison to the radar retrievals at low IWC values) than IWCs calculated using Brown and Francis (1995).

The mixed-phase cloud optical depth maximum is about 18, and is almost entirely determined by the liq-

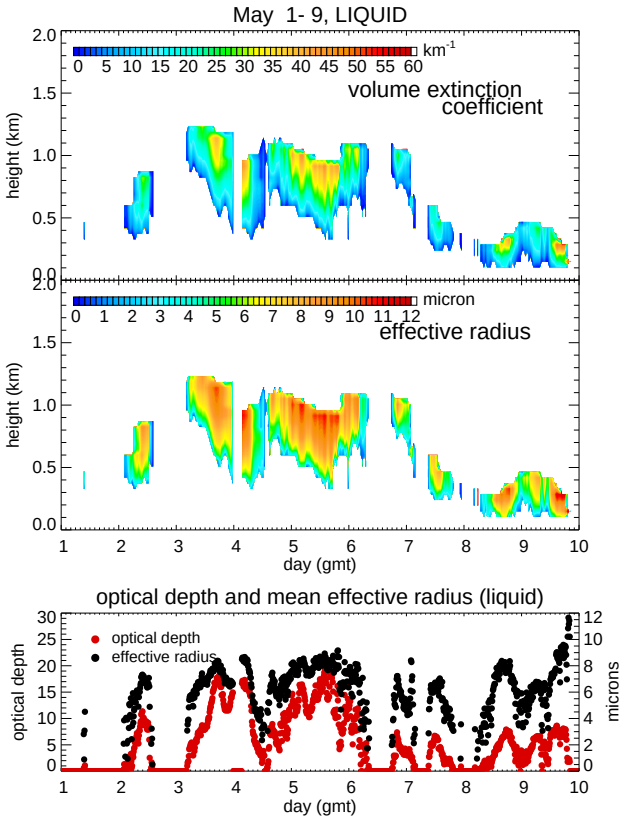

FIG. 6: Similar to Fig. 5 but for the liquid component, and including the liquid effective radius. Note the change in vertical scale.

uid component. Large decreases in cloud optical depth accompany the presence of upper ice clouds, which can sediment ice crystals into the lower cloud and uptake its water. The liquid component reasserts itself when no upper clouds are present.

This retrieval technique should apply whenever the liquid water paths exceed their error estimate of about 25 g m^{-2} (Westwater et al., 2001). Mixed-phase cloud conditions with low liquid water paths may be more common, and for such clouds, a different characterization of the liquid component is needed. Future work will examine the aircraft and remote sensor data for other mixed-phase clouds observed during FIRE/ACE. A more in-depth analysis of this case will be presented at the conference.

Acknowledgments The first author was supported by a National Research Council Research Associateship Award.

REFERENCES

Alvarez, R., W. Eberhard, J. Intrieri, C. Grund, and S. Sandberg, 1998: A depolarization and backscatter lidar for unattended operation in varied meteorological conditions. *10th AMS Symp. on Met. Obs. Instr.* Jan. 11–16 Phoenix, AZ.

Baker, B., C. Schmitt, P. Lawson, and D. Mitchell, 2002: Further analysis and improvements of ice crystal mass-size relationships. *11th AMS Conference on Cloud Physics* 3–7 June, Ogden, UT.

Bradley, R., F. Keimig, and H. Diaz, 1993: Recent changes in the North American Arctic boundary layer in winter. *J. Geophys. Res.*, **98**, 8851–8858.

Brown, P. R. A. and P. N. Francis, 1995: Improved measurements of the ice water content in cirrus using a total-water probe. *J. Atmos. Oceanic. Tech.*, **12**, 410–414.

Hogan, R., P. Francis, H. Flentje, A. Illingworth, M. Quante, and J. Pelon, 2002: Characteristics of mixed-phase clouds part I: Lidar, radar and aircraft observations from CLARE '98. *Q. J. R. Meteorol. Soc.*, **128**, 28 pp.

Intrieri, J. and M. Shupe, 2002: Sensitivity of surface cloud radiative forcing to Arctic cloud properties. *11th AMS Conf. on Atm. Rad.* Ogden, UT, 3–7 June 2002.

Intrieri, J., M. Shupe, T. Uttal, and B. McCarty, 2002: An annual cycle of Arctic cloud characteristics observed by radar and lidar at SHEBA. *J. Geophys. Res.*, **107**, (C10) 10.1029/2000JC000423.

Lawson, R., B. A. Baker, C. G. Schmitt, and T. L. Jensen, 2001: An overview of microphysical properties of Arctic clouds observed in May and July 1998 during FIRE ACE. *J. Geophys. Res.*, **106**, 14,989–15,014.

Matrosov, S., A. V. Korolev, and A. J. Heymsfield, 2002: Profiling cloud ice mass and particle characteristic size from doppler radar measurements. *J. Atmos. Ocean. Tech.*, **19**, 1003–1018.

Matrosov, S., M. Shupe, A. J. Heymsfield, and P. Zuidema, 2003: Ice cloud optical thickness and extinction estimates from radar measurements. *J. Appl. Meteorol.* submitted.

Moran, K. P., B. E. Martner, M. J. Post, R. Kropfli, D. C. Welsh, and K. B. Widener, 1998: An unattended cloud-profiling radar for use in climate research. *Bull. Amer. Meteorol. Soc.*, **79**, 443–455.

Rogers, R. R. and M. K. Yau, 1989: *A Short Course in Cloud Physics*. Pergamon Press, 293.

Shupe, M. D., T. Uttal, S. Matrosov, and A. S. Frisch, 2001: Cloud water contents and hydrometeor sizes during the FIRE-Arctic Clouds Experiment. *J. Geophys. Res.*, **106**, 15,015–15,028.

Stone, R., 1997: Variatons in western arctic temperatures in response to cloud radiative and synoptic-scale influences. *J. Geophys. Res.*, **102**, 21769–21776.

Uttal, T. and . co authors, 2002: Surface heat budget of the Arctic ocean. *Bull. Amer. Meteorol. Soc.*, **83**, 255–275.

Westwater, E. R., Y. Han, M. D. Shupe, and S. Y. Matrosov, 2001: Analysis of integrated cloud liquid and precipitable water vapor retrievals from microwave radiometers during the Surface Heat Budget of the Arctic Ocean project. *J. Geophys. Res.*, **106**, 32,019–32,030.